Development of Sol–Gel Derived SiO_2-TiO_2 Double Layer Antireflective Coatings for Solar Glass Covers

Sandip S. Patil[1], Renuka A. Pawar[2]
[1,2]*Shri Vijaysinha Yadav College, Pethvadgaon*
doi.org/10.64643/IJIRTV13I4-208071-459

***Abstract*—Solar glass covers play a critical role in determining the energy conversion efficiency of photovoltaic modules and solar thermal systems. However, significant reflection losses at the glass interface remain a barrier to maximizing sunlight collection. In this study, we fabricated highly transparent double-layer TiO_2-SiO_2 antireflective coatings via a simple, scalable base-catalyzed sol–gel method combined with dip-coating. Methyltriethoxysilane (MTES) was used to introduce a nanoporous structural network in the top silica layer to effectively lower its refractive index, while titanium (IV) isopropoxide (TTIP) served as the precursor for a dense underlying titania layer. Fourier transform infrared spectroscopy (FTIR) confirmed the successful chemical integration of the two metal oxides through the distinct formation of interfacial Si–O–Ti heterolinkages, alongside the preservation of hydrophobic methyl Si–CH_3 functional groups from the chemical modifier. Scanning electron microscopy (SEM) micrographs revealed that sequentially depositing the low-index SiO_2 outer layer successfully filled in microscopic valley regions and localized thermal stress cracks present on the underlying titania base layer, creating an exceptionally smooth and continuous bilayer surface. This optimized microstructural stack significantly suppressed surface light-scattering defects. Consequently, UV-Vis transmittance spectra demonstrated excellent broadband antireflective performance, achieving a peak transmittance of ~98.8% around 530 nm compared to the single-layer configurations. These findings highlight a practical, cost-effective path toward developing durable, high-efficiency optical coatings for long-term outdoor solar energy harvesting applications.**

***Index Terms*—Antireflective coatings; Sol–gel process; Double-layer coatings; SiO_2–TiO_2 hybrid; Transmittance; Surface morphology.**

I. INTRODUCTION:

Solar glass covers are a key component in photovoltaic (PV) modules and solar thermal collectors because they directly influence how much sunlight reaches the active surface. To minimize reflection losses and improve energy conversion efficiency, anti-reflective coatings (ARCs) [1-3] are commonly applied not only to solar glass [4,5] but also to automobile windshields [6-7] and architectural glazing.[8] Several fabrication methods have been developed for producing these coatings, such as sputtering [9], chemical vapor deposition (CVD) [10], and the sol–gel technique [11]. Among these approaches, the sol–gel process has become the preferred option for large-scale manufacturing due to its relatively low cost, simple processing, and suitability for industrial production.

Sol–gel-derived ARCs can be synthesized through either acid-catalyzed or base-catalyzed reactions, with each route producing coatings that possess different characteristics. Acid-catalyzed coatings generally exhibit good mechanical integrity because of their dense structure. However, their relatively low porosity leads to a higher refractive index, which limits their antireflective performance. [12] In contrast, base-catalyzed coatings develop a porous silica network that lowers the refractive index and significantly improves light transmission. Despite this optical advantage, the porous framework contains numerous hydroxyl groups that readily interact with moisture, making these coatings vulnerable to humidity. As a result, conventional base-catalyzed ARCs often show inadequate mechanical durability and poor resistance to long-term outdoor weathering.

To address these shortcomings, researchers have explored various post-synthesis surface modification

techniques aimed at improving both durability and self-cleaning behavior. One widely adopted approach involves treating the coating with ammonia, followed by exposure to hexamethyldisilazane (HMDS) or hexamethyldisiloxane vapor. This treatment replaces reactive surface hydroxyl groups with hydrophobic functional groups, reducing moisture adsorption and improving resistance to environmental contamination. Such modifications help maintain the transparency of porous silica coatings by limiting dirt accumulation and reducing optical degradation during prolonged heating. Nevertheless, outdoor solar glass is exposed to more than just humidity and elevated temperatures. Rainwater, which often contains dissolved salts, repeatedly washes over the surface. As the water evaporates, salt deposits remain behind, lowering light transmission and, over extended periods, potentially accelerating surface corrosion. Although several studies have reported coatings that combine antireflective and self-cleaning functions, questions remain regarding their long-term thermal stability and environmental durability under realistic service conditions.

In the present work, highly transparent antireflective coatings were fabricated using a base-catalyzed sol–gel process. The coating thickness and refractive index were carefully optimized by adjusting the sol concentration and aging time to achieve minimum reflectance.

II. MATERIALS AND METHODS

2.1. Materials and Substrate Preparation

Tetrabutyl titanate (TBT, 99%), Methyltrimethoxysilane (MTMS, 99%), hydrochloric acid (HCl, 37%), anhydrous ethanol, and deionized water were used as the starting materials for this work. All chemicals were of analytical grade and used without further purification.

Glass slides served as the substrates for thin-film deposition. Before coating, each slide was cleaned thoroughly to eliminate surface contaminants that could affect film quality. The cleaning procedure began with washing the slides in a detergent solution, followed by immersion in nitric acid. The substrates were then rinsed several times with deionized water and ultrasonically cleaned for 10 min. A second ultrasonic cleaning step was carried out in acetone for another 10 min to remove any remaining organic residues. Finally, the slides were rinsed with fresh deionized water and kept immersed until they were used for film deposition.

2.2. Preparation of Single-Layer TiO_2 Coatings

Titanium dioxide sol was prepared using titanium(IV) isopropoxide (TTIP, 97%) as the titanium precursor. Initially, 10 mL of TTIP was dissolved in 100 mL of absolute ethanol under continuous magnetic stirring. To control the hydrolysis reaction and prevent rapid precipitation, 15 g of 5 wt% hydrochloric acid solution was added slowly, dropwise, while maintaining vigorous stirring. The solution was stirred for approximately 45 min until a clear and homogeneous sol was obtained and subsequently aged at room temperature for 12 h before coating.

The cleaned glass substrates were coated by the dip-coating technique. Each substrate was immersed vertically into the TiO_2 sol and withdrawn at a controlled speed using a motorized dip coater. After deposition, the films were dried in ambient air for approximately 10 min to allow solvent evaporation.

The coated substrates were annealed at 150 °C for 1 h in a muffle furnace and then allowed to cool naturally inside the furnace to room temperature, resulting in transparent and uniform TiO_2 coatings. Single-layer TiO_2 coatings were prepared by keeping the withdrawal speed at 2.0 mm s^{-1} during dip coating.

2.3. Preparation of Single-Layer SiO_2 Coatings

A silica sol was prepared using methyltriethoxysilane (MTES, 98%) as the silica precursor. Initially, 5 mL of MTES was mixed with 104 mL of anhydrous ethanol under continuous magnetic stirring until a clear solution was obtained. To initiate the hydrolysis reaction while preventing rapid condensation, 12.2 g of 6.7 wt% hydrochloric acid solution was added dropwise under vigorous stirring. The resulting mixture was stirred for approximately 45 min, followed by aging at room temperature for 12 h to obtain a stable, homogeneous sol suitable for dip coating.

The cleaned glass substrates were vertically immersed in the prepared sol and withdrawn at predetermined speeds using a motorized dip-coating unit. After deposition, the coated substrates were dried in air for approximately 10 min to allow solvent evaporation. The films were then annealed at 150 °C

for 1 h in a muffle furnace and cooled naturally to room temperature inside the furnace. This procedure produced transparent, uniform, and well-adhered SiO_2 coatings. Single-layer SiO_2 coatings were prepared by keeping the withdrawal speed of 2.04 mm s^{-1} during dip coating.

2.4. Preparation of TiO_2/SiO_2 Double-Layer Coatings:

TiO_2/SiO_2 double-layer coatings were fabricated by sequential deposition of TTIP-derived TiO_2 and MTES-derived SiO_2 layers using the dip-coating technique. Initially, the TiO_2 layer was deposited onto the cleaned glass substrate and pre-heated at 90 °C for 15 min to remove residual solvent and improve film adhesion.

After cooling to room temperature, the MTES-derived SiO_2 sol was deposited over the TiO_2 layer to form the outer antireflective coating. The bilayer-coated substrates were again pre-heated at 90 °C for 15 min, followed by final annealing at 150 °C for 1 h. The samples were then cooled gradually inside the furnace to room temperature. A TiO_2-SiO_2 double-layer coatings were prepared by keeping the withdrawal speeds of 0.98 mm s^{-1}.

III. RESULT AND DISCUSSION

3.1 FTIR Analysis

Fourier transform infrared (FTIR) spectroscopy was used to investigate the chemical bonding and structural composition of the pure SiO_2, pure TiO_2, and binary SiO_2–TiO_2 hybrid coatings. Figure 1 shows the recorded spectra between 4000 cm^{-1} and 500 cm^{-1}, and the specific peak assignments are summarized in Table 1.

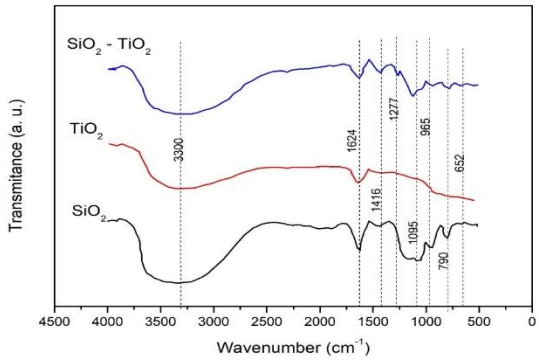

Fig 1: FTIR spectra of SiO_2, TiO_2 and TiO_2 – SiO_2 hybrid coatings

Hydroxyl Region	Organic Modifier	Inorganic Framework
(3500–1600 cm^{-1})	(1450–1250 cm^{-1})	(1100–600 cm^{-1})
• O–H Stretch (3300)	• C–H Bending (1416)	• Si–O–Si Stretch (1095)
• H_2O Bending (1624)	• Si–CH_3 Bending (1277)	• Si–O–Ti Network (965)
		•Ti–O–Ti Framework (652)

Table: FTIR data of SiO_2, TiO_2 and TiO_2 – SiO_2 hybrid coatings

All three samples display a very broad absorption band centered around 3300 cm^{-1}. This broad feature belongs to the stretching vibrations of O–H groups, [13] which come from surface silanols (Si–OH), titanols (Ti–OH), and physically adsorbed water molecules. Another common eature is the sharp peak at 1624 cm^{-1}, which represents the (O–H) bending vibration of water [14] trapped inside the gel networks. The presence of these peaks across all samples is typical for sol-gel derived oxide materials.

Looking at the spectra for pure SiO_2 and the TiO_2 – SiO_2 composite, we can clear see two peaks at 1416 cm^{-1} and 1277 cm^{-1} that do not appear in the pure TiO_2 sample. The peak at 1416 cm^{-1} is due to the asymmetric bending of C–H bonds in the –CH_3 groups. [15] The sharp, strong peak at 1277 cm^{-1} is the symmetric bending of C–H directly attached to silicon (Si–CH_3). [16] These peaks confirm that the methyl groups from the MTMS precursor successfully integrated into the silica-containing networks and survived the processing steps.

The fingerprint region below 1200 cm^{-1} shows how the inorganic networks actually formed. For the pure SiO_2 coating, the most intense peak shows up at 1095 cm^{-1}, which is the asymmetric stretching of the main Si–O–Si network. [17] A smaller peak at 790 cm^{-1} matches the symmetric stretching of cyclic siloxane structures. [18] For pure TiO_2, these silica peaks are missing, and we instead see a broad absorption band starting below 800 cm^{-1} and peaking around 652 cm^{-1} which represents the continuous Ti–O–Ti lattice. [19, 20]

The most important evidence for the hybrid TiO_2–SiO_2 coating is the peak around 965 cm^{-1}. [21] In pure silica, this region usually just shows a small shoulder from stretching defects Si–OH non-bridging oxygen atoms). However, in the hybrid sample, this band becomes significantly broader and stronger. This clear change confirms the formation of true Si–O–Ti cross-linkages, proving that the silica and titania did not just mix mechanically but actually bonded chemically at the interface.

The FTIR data shows that the sol-gel process successfully created a co-continuous network. The presence of Si–O–Si Ti–O–Ti, and interfacial Si–O–Ti bonds confirm successful chemical integration of the two oxides. At the same time, the remaining Si–CH peaks show that the organic modification was preserved, which is expected to influence the final surface properties of the hybrid coating.

3.2 Surface Morphology and Microstructure (SEM Analysis)

The microstructural evolution and surface topologies of the thin-film configurations were examined using scanning electron microscopy (SEM) to understand how structural arrangements impact the overall optical transmittance.

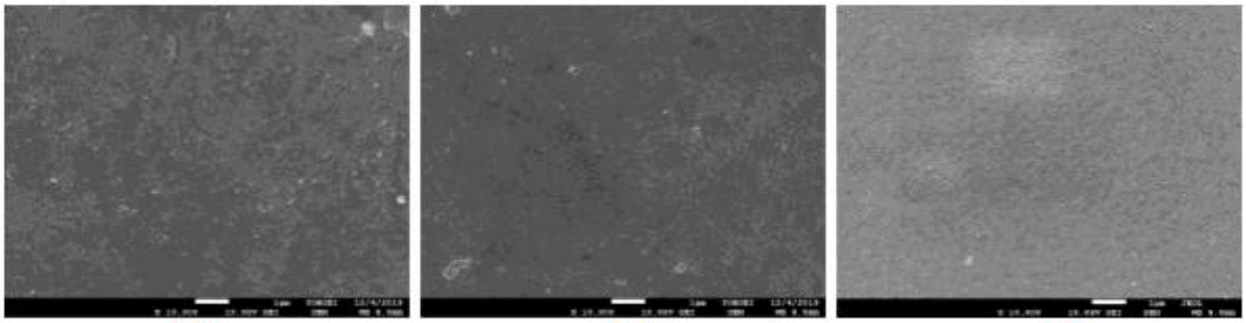

Fig. 2: Scanning electron micrograph of (a) TiO_2, (b) SiO_2, and (c) TiO_2–SiO_2 coatings

The Pristine TiO_2 Layer (Figure 2a): This micrograph reveals a generally uniform, highly dense matrix, which is expected due to the structural compaction typical of pure titania sol-gel films. However, the surface exhibits isolated patch-like micro-domains characterized by tightly packed nanoscale cracking. These features likely stem from thermal stress accumulation during the 150 °C calcination step, where the evaporation of residual solvents forces network contraction. The highly dense nature of this continuous layer underpins its relatively high refractive index profile.

The Pure SiO_2 Layer (Figure 2b): In stark contrast, the silica film demonstrates a distinct, granular morphology dominated by a finely interconnected network. This nanoporous architecture is a direct product of the base-catalyzed condensation pathways, where discrete silica clusters cluster together rather than forming a fully dense mass. The visible, well-distributed porosity throughout this matrix explains its ability to lower the refractive index, acting as the primary driver behind the high optical transmittance observed in the single-layer silica specimen.

The Combined TiO_2–SiO_2 System (Figure 2c): When the low-index SiO_2 top layer is sequentially deposited over the high-index TiO_2 base film, the surface appearance changes dramatically. The sharp granular structures and the localized stress-cracking domains seen in the single layers are no longer prominent. Instead, the micrograph shows a highly smooth, continuous, and homogeneous topography.

This structural smoothing indicates that the freshly applied overlayer fills in any micro-voids, cracks, or valley regions present on the underlying titania base layer during the dip-coating withdrawal process. This structural filling yields a well-integrated, cohesive bilayer stack. [1, 2]

From an optical perspective, this smooth and defect-free surface is excellent for solar panel glass covers. Eliminating large surface defects and cracks suppresses unwanted diffuse scattering losses at the air-coating interface. Consequently, it allows the destructive interference mechanics of the double-layer stack to operate optimally, guiding more photons through the glass substrate and explaining

the superior transmittance (~98.8%) achieved by this sample.

3.3. UV-Vis Transmittance Analysis:

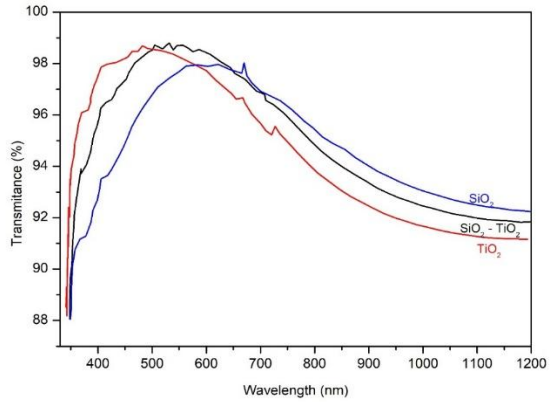

Fig. 3: UV-Vis spectrograph of TiO_2, SiO_2, and TiO_2–SiO_2 coatings

To see how well our coatings actually reduce reflection, we measured their UV-Vis transmittance spectra between 350 and 1200 nm. Figure 2 shows the light transmission curves for our single-layer TiO_2, single-layer SiO_2, and the double-layer SiO_2-TiO_2 coating.

The silica layer SiO_2, this film gives a maximum transmittance of ~98.0% around 580 nm. The broad high transparency across the visible spectrum makes sense because the porous silica structure has a low refractive index. [22]

The titania layer TiO_2, this sample reaches its peak transmission of ~98.6% near 480–500 nm. However, if we look closely at the ultraviolet region below 400 nm, the transmittance drops off sharply. This sudden drop is expected because of the intrinsic UV absorption caused by the bandgap of TiO_2.

When we look at the double-layer SiO_2–TiO^2 system, it clearly shows the best optical performance for solar panel covers. The maximum transmittance improves to ~98.8% around 530 nm. Instead of a narrow peak, it maintains a wider, more stable flat transmission profile across the main visible light range. This happens because we paired a high-refractive-index bottom layer TiO_2 with a low-refractive-index top layer SiO_2, creating a classic optical stack. By adjusting the thickness, the reflections coming off the different boundaries undergo destructive interference and cancel each other out. Because less light is reflected away, more photons can pass directly through the glass. This broad, high-transmission behavior is exactly what we need to increase the light-harvesting efficiency of underlying solar cells.

IV. CONCLUSION

In conclusion, high-transmittance TiO_2-SiO_2 double-layer antireflective coatings were successfully developed on glass substrates using a base-catalyzed sol–gel approach followed by a controlled dip-coating process. Our systematic analysis confirms the following key findings:

FTIR analysis verified that the composite network was not a simple physical mixture. The noticeable broadening of the peak at 965 cm^{-1} confirmed that the SiO_2 and TiO_2 phases bonded chemically at their boundaries to produce robust cross-linked Si–O–Ti networks, while preserving the organic methyl group profiles Si–CH_3 at 1277cm^{-1} necessary for tailored surface behavior.

SEM tracking revealed a significant structural modification. The application of the outer silica layer acted as an interfacial filler that filled localized thermal stress defects and boundary voids present on the pure titania film, shifting the surface configuration from an isolated cracked network into a highly uniform, smooth, and defect-free bilayer top coat.

Due to this structural smoothing and the destructive optical interference created by pairing the high-index TiO_2 base layer with the low-index SiO_2 overlayer, reflection losses were heavily minimized. The double-layer coating achieved an exceptional maximum visible light transmittance of ~98.8% at 530 nm and displayed a notably broad, flat transmission window compared to individual single layers.

Taken together, these results show that tuning the structural and chemical interactions within a basic layered metal-oxide matrix can produce high-efficiency optical components. This study offers a simple and reproducible coating architecture highly suited for improving the light-harvesting output of commercial solar energy devices

REFERENCES

[1] Raut, H.K., Ganesh, V.A., Nair, A.S. and Ramakrishna, S., 2011. Anti-reflective coatings:

A critical, in-depth review. Energy & Environmental Science, 4(10), pp.3779-3804.

[2] Moayedfar, M. and Assadi, M.K., 2018. Various types of anti-reflective coatings (ARCS) based on the layer composition and surface topography: a review. Reviews on Advanced Materials Science, 53(2), pp.187-205.

[3] Shanmugam, N., Pugazhendhi, R., Madurai Elavarasan, R., Kasiviswanathan, P. and Das, N., 2020. Anti-reflective coating materials: A holistic review from PV perspective. Energies, 13(10), p.2631.

[4] Law, A.M., Jones, L.O. and Walls, J.M., 2023. The performance and durability of Anti-reflection coatings for solar module cover glass–a review. Solar Energy, 261, pp.85-95.

[5] Priyadarshini, B.G. and Sharma, A.K., 2016. Design of multi-layer anti-reflection coating for terrestrial solar panel glass. Bulletin of Materials Science, 39(3), pp.683-689.

[6] Choi, T.H., Lee, H.W. and Ha, J.U., 2023. Light control using vertically aligned dichroic dye films for windshield antireflection in automotive displays. Applied Optics, 62(3), pp.584-591.

[7] Song, J., Kim, H.S. and Park, J., 2025. Predictive modeling and evaluation of LiDAR sensors through automotive windshields with anti-reflective coatings. Results in Engineering, p.107000.

[8] Anderson, A.L., Chen, S., Romero, L., Top, I. and Binions, R., 2016. Thin films for advanced glazing applications. Buildings, 6(3), p.37.

[9] Jeong, S.H., Kim, J.K., Kim, B.S., Shim, S.H. and Lee, B.T., 2004. Characterization of SiO2 and TiO2 films prepared using rf magnetron sputtering and their application to anti-reflection coating. Vacuum, 76(4), pp.507-515.

[10] Shanmugam, N., Pugazhendhi, R., Madurai Elavarasan, R., Kasiviswanathan, P. and Das, N., 2020. Anti-reflective coating materials: A holistic review from PV perspective. Energies, 13(10), p.2631.

[11] Prado, R., Beobide, G., Marcaide, A., Goikoetxea, J. and Aranzabe, A., 2010. Development of multifunctional sol–gel coatings: Anti-reflection coatings with enhanced self-cleaning capacity. Solar Energy Materials and Solar Cells, 94(6), pp.1081-1088.

[12] Vincent, A., Babu, S., Brinley, E., Karakoti, A., Deshpande, S. and Seal, S., 2007. Role of catalyst on refractive index tunability of porous silica antireflective coatings by sol− gel technique. The Journal of Physical Chemistry C, 111(23), pp.8291-8298.

[13] Shabanian, M., Hajibeygi, M. and Raeisi, A., 2020. FTIR characterization of layered double hydroxides and modified layered double hydroxides. In Layered double hydroxide polymer nanocomposites (pp. 77-101). Woodhead Publishing.

[14] Pogorelov, V., Doroshenko, I., Pitsevich, G., Balevicius, V., Sablinskas, V., Krivenko, B. and Pettersson, L.G., 2017. From clusters to condensed phase–FT IR studies of water. Journal of Molecular Liquids, 235, pp.7-10.

[15] Karabacak, M., Çoruh, A. and Kurt, M., 2008. FT-IR, FT-Raman, NMR spectra, and molecular structure investigation of 2, 3-dibromo-N-methylmaleimide: A combined experimental and theoretical study. Journal of Molecular Structure, 892(1-3), pp.125-131.

[16] Ferguson, G.A. and Raghavachari, K., 2006. The emergence of collective vibrations in cluster models: Quantum chemical study of the methyl-terminated Si (111) surface. The Journal of chemical physics, 125(15).

[17] Liu, H., Kaya, H., Lin, Y.T., Ogrinc, A. and Kim, S.H., 2022. Vibrational spectroscopy analysis of silica and silicate glass networks. Journal of the American Ceramic Society, 105(4), pp.2355-2384.

[18] Yoshino, H., Kamiya, K. and Nasu, H., 1990. IR study on the structural evolution of sol-gel derived SiO2 gels in the early stage of conversion to glasses. Journal of Non-Crystalline Solids, 126(1-2), pp.68-78.

[19] Alotaibi, M.A., Alharthi, A.I., Qahtan, T.F., Alotibi, S., Ali, I. and Bakht, M.A., 2024. Green synthesis of xanthene derivatives through visible light-driven photocatalysis using blackberry dye-sensitized TiO2. Journal of Alloys and Compounds, 978, p.173388.

[20] Gao, X., Bare, S.R., Fierro, J.L.G., Banares, M.A. and Wachs, I.E., 1998. Preparation and in-situ spectroscopic characterization of molecularly dispersed titanium oxide on

silica. The Journal of Physical Chemistry B, 102(29), pp.5653-5666.

[21] Landmann, M., Köhler, T., Rauls, E., Frauenheim, T. and Schmidt, W.G., 2014. The atomic structure of ternary amorphous Ti x Si1− x O2 hybrid oxides. Journal of Physics: Condensed Matter, 26(25), p.253201.

[22] Krishnan, M.R., Rajendran, V. and Alsharaeh, E., 2023. Anti-reflective and high-transmittance optical films based on nanoporous silicon dioxide fabricated from templated synthesis. Journal of Non-Crystalline Solids, 606, p.122198.